Impact of the radiative forcing on the winter North Atlantic-European atmospheric circulation

Author: Mireia Ginesta Fernandez
Supervisors: [1]Javier García Serrano and [2]Guillaume Gastineau
[1]*Facultat de Física, Universitat de Barcelona, Diagonal 645, 08028 Barcelona, Spain. and*
[2]*LOCEAN-IPSL, Sorbonne Universités/CNRS/IRD/MNHN, Paris, France*

Abstract: The increase in the global-mean temperature linked to climate change is associated with atmospheric and oceanic circulation changes. In this work, we assess the impacts of the (anthropogenic) radiative forcing on the North Atlantic-European atmospheric circulation during boreal winter (DJF). We use two approaches: three target experiments with the European Consortium – Earth System model version 3.3 (EC-EARTH) and fixed radiative forcing, and three large-ensemble historical/scenario simulations with the Institut Pierre-Simon Laplace Coupled Model version 6 (IPSL-CM6), characterizing Past, Present-day and near-Future climate conditions. First, a comparison between the Present simulations and observations shows that both models simulate a too zonal eddy-driven jet. Then, differences between the radiative forcings are analysed. Results show that both approaches yield a consistent forced response, and that it scales linearly with radiative forcing, increasing in amplitude from Present-minus-Past to Future-minus-Present. At low latitudes, in the tropical Atlantic, the forced atmospheric response is characterized by a Gill-type baroclinic structure, where the anomalous anticyclonic circulation at upper levels reinforces the westerly wind at the equatorward flank of the North Atlantic jet. At high latitudes, the forced response is reminiscent of the 'Arctic Amplification' linked to sea-ice reduction, and a thermally-driven baroclinic structure can be seen west of Greenland (EC-EARTH) and over the Hudson Bay (IPSL). At mid-latitudes, the forced response shows a barotropic pattern, with a cyclonic (anticyclonic) circulation in the North Atlantic (Euro-Mediterranean) sector, pointing to a key role for non-radiative, eddy-related effects.

I. INTRODUCTION

The accelerated global warming linked to climate change has become a topic of great interest due to its projected impact on ecosystems. This warming owes its existence to human-induced radiative forcing, also known as anthropogenic radiative forcing, that results from an increase in concentration of the principal greenhouse gases (GHGs) such as carbon dioxide (CO_2), methane (CH_4), chlorofluorocarbons ($CFCs$) and nitrous oxide (N_2O), as well as aerosols and land-use changes (*Houghton et al.* 2001). Among other effects, the anomalous increase in global temperature is expected to yield oceanic and atmospheric circulation changes.

The atmospheric circulation in the troposphere is composed of a mean meridional circulation, climatological or stationary waves, and transient eddies. The mean meridional circulation is the time-averaged and zonally-averaged flow, and is mainly characterized by the Hadley and Ferrel cells. The Hadley cell, which is a thermally-direct circulation, is linked to the subtropical jet as a consequence of the angular momentum conservation on its upper branch. Stationary waves are zonal deviations of the time-averaged flow, and they emerge from the longitudinal asymmetry of the land-sea interface, that is, variations in surface elevation and surface temperature throughout a latitudinal band. Transient eddies are temporal and zonal deviations from the time-averaged and zonally-averaged flow. These eddies represent extra-tropical cyclones and anticyclones that characterize the synoptic-scale circulation at mid-latitudes. Stationary waves and transient eddies, especially the latter, play an essential role in climate dynamics transporting energy, mostly as sensible heat, polewards. They also transport moisture and westerly momentum, e.g. giving rise to the eddy-driven jet. Wave activity is much stronger in the winter hemisphere, when the solar radiation reaches its minimum at the pole and generates a strong meridional gradient between low and high latitudes. In this project, we focus on the mean atmospheric circulation changes under different radiative forcings in the North Atlantic-European (NAE) winter (December-January-February, hereafter DJF).

Figure 1 shows an schematic of the NAE atmospheric circulation during DJF. In the tropical Atlantic, a subtropical jet is well-distinguished over Africa that extends over the eastern Atlantic (Fig. 1 black contours). The North Atlantic jet, separated from the African jet and generated at the eastern coast of the United States, has a thermally-driven component at its entrance over south-eastern North America but it is eddy-driven at its core over the Atlantic ocean. A key difference between the two jets relies on their vertical structure. The subtropical jet has a baroclinic structure, with lower-level easterlies and upper-level westerlies. In contrast, the eddy-driven component of the North Atlantic jet has a barotropic structure, with westerlies throughout the vertical column (e.g. *Woollings* 2010). At mid-latitudes, weather and climate are highly influenced by the storm tracks (Fig. 1 black arrow), which are the preferred regions where extra-tropical cyclones originate, travel, and dissipate. They are generated in regions of strong baroclinicity, which are regions

with a strong meridional temperature gradient [(1) in Fig. 1] (*Holton*). These are associated with the western boundary currents, such as the Gulf Stream in the North Atlantic, which sharply separate warm waters to the south and cold waters to the north (*Brayshaw et al.* 2009), strengthened during boreal winter. In their development, cyclones travel downstream interacting with the mean flow and converting potential energy into kinetic energy by means of barotropic processes, setting the eddy-driven jet by westerly momentum convergence [(2) in Fig. 1]. Momentum deposition, non-linear interactions, and surface friction, among other factors, dissipate the eddies, whose life ends at the storm-track exit region [(3) in Fig. 1]. The climatological configuration of the storm tracks and eddy-driven jet helps settling a surface pressure dipole between the semipermanent Icelandic Low and Azores High [L and H in Fig. 1, respectively]. Relative changes between these centres of surface pressure are known as the see-saw that characterizes the North Atlantic Oscilation (NAO).

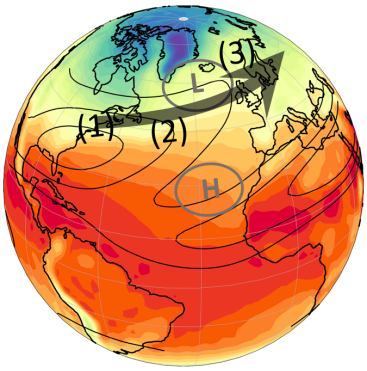

FIG. 1. Schematic of the main features of the North Atlantic-European atmospheric circulation during DJF: the storm track (black arrow), zonal wind at 200hPa (contours every 10 m/s from 20m/s to 40m/s), the climatological low (L) and high (H) pressure systems, and 2-metre air temperature (shading every 2K from 248K to 304K). Data from the ERA5 reanalysis.

Modelling the response of the extratropical atmospheric circulation to anthropogenic climate change is quite challenging, specially in the NAE region, as it depends on many dynamical and thermodynamical factors. A key modulator of the North Atlantic storm track and eddy-driven jet is via changes in the meridional temperature gradient and related baroclinicity. Under climate change, two opposing influences are projected to modify baroclinicity: the tropical upper-tropospheric warming (UTW) and the Arctic warming amplification (AA). UTW is mainly due to an increase in latent heat release at upper-levels: as temperature increases, saturation vapor pressure increases according to the Clausius-Clapeyron relation, hence, the low-level air is moister resulting in more condensation and latent heat release (e.g. *Shaw et al.* 2016). Arctic amplification, also known as polar amplification, results from the interaction of many feedbacks, including the albedo feedback, namely a positive feedback that increases absorbed solar radiation due to sea ice loss and the associated reduction in albedo (*Serreze and Francis* 2006). UTW and AA have opposing effects on the storm tracks. UTW enhances the upper-level meridional temperature gradient, and a poleward shift of the storm tracks is expected. Conversely, AA reduces the lower-level meridional temperature gradient, in principle weakening and shifting equatorward the storm tracks. *Woollings et al.* (2012) show that the North Atlantic storm track projection with climate change consists of a strengthening and eastward extension to Europe, with the Atlantic Meridional Overturning Circulation (AMOC) slowdown playing an important role. Other studies project an increase in extratropical cyclone activity over the northeastern North Atlantic and western Europe (*Shaw et al.* 2016). Together, this is somehow consistent with the multi-model study by *Zappa et al.* (2012) using Coupled Model Intercomparison Project phase 5 (CMIP5), which shows that the storm track response consists of a tripolar pattern: a small increase in storm activity over the British Isles, a reduction over the Norwegian Sea and a large reduction over the Mediterrenean Sea.

Climate projections have large uncertainties that arise mainly from an incomplete knowledge of the radiative forcing (e.g. GHG concentrations, aerosols and land-uses), model uncertainty (e.g. physical and numerical formulations), and internal variability (*Deser et al.* 2012). Internal variability, also called 'climate noise', constitutes natural oscillations within the climate system linked to the mutual interaction of its different components, and whose low-frequency phase depends mainly on the initial condition of the climate simulations. Identifying the human-induced changes in the climate state requires to separate this forced signal from the internal, unforced variability, and usually requires a large sampling (*Deser et al.* 2020).

We tackle this challenge following two approaches: on one hand, we use three 240-year long sensitivity experiments with fixed radiative forcing, performed with EC-EARTH; on the other hand, we employ three large-ensemble historical/scenario simulations performed with IPSL-CM6. In both cases, the radiative forcing is representative of past, present and future climate conditions. Details are provided in Section II. In the Results section (III), the performance of both models is first assessed in present climate and compared to observations; then, the response to radiative forcing is explored with respect to past and future climate. Finally, Section IV summarizes the conclusions of this work.

II. METHODOLOGY

A. MODELS AND OBSERVATIONAL DATA

In this study we use observationally constrained data as a proxy for the true state of the atmosphere. We use 30 winters from December 1979 to February 2010 of the **ERA5** reanalysis from the European Centre for Medium-Range Weather Forecasts (ECMWF) atmospheric reanalysis, which has a horizontal resolution of 31km (*Hersbach et al.* 2020).

To isolate the response to radiative forcing, we have used two approaches, whose simulations follow the historical and Shared Socioeconomic Pathway 2-4.5 (SSP2-4.5) radiative forcing from CMIP6 (*O'Neill et al.* 2016). The first approach consists of three 240-year simulations performed with the European Consortium – Earth System model version 3.3 (**EC-EARTH**) keeping fixed the radiative forcing, that is, fixed concentration of greenhouse gases and aerosols, at 1950, characterizing the Past climate, at 2000, representative of Present-day conditions, and at 2050, projecting the near-Future climate. In these simulations, the response to anthropogenic radiative forcing is isolated and the internal variability or 'noise' is filtered out as a consequence of having enough sampling. The second approach makes use of the initial-condition Large Ensemble (i.e. 32 members, here we only use 24 members) of transient simulations performed with IPSL-CM6A-LR, the latest version of the Institut Pierre-Simon Laplace Climate Model (**IPSL**) (*Boucher et al.* 2020). Three 10-year periods have been considered, in order to have the same size of sampling than for EC-EARTH simulations (24 members x 10 years each), namely 1949-1959, 1999-2009, and 2049-2059. Here, the anthropogenic radiative forcing is assumed to be relatively constant. The internal variability, which is randomly phased out between ensemble members, can be largely reduced by computing the ensemble-mean (*Deser et al.* 2020). An schematic of the experimental set-up used in this work is shown in Fig. 2, using the CO2 concentration from another Earth system model (*Meinshausen et al.* 2020), although it is representative of the full radiative forcing applied, including other GHGs and aerosols (*O'Neill et al.* 2016).

For the atmospheric component, EC-EARTH uses the Integrated Forecast System (IFS) model, with a horizontal spectral resolution of T255 (triangular truncation at wavenumber 255; 512x256 lonxlat) and 91 vertical levels up to 0.01hPa. On the other hand, IPSL uses the LMDZ model, developed at Laboratoire de Météorologie Dynamique, with a horizontal resolution of 143x144 (lonxlat) and 79 vertical levels up to 80km. Both coupled models use the Nucleus for European Modeling of the Ocean (NEMO) version 3.6 for the oceanic component.

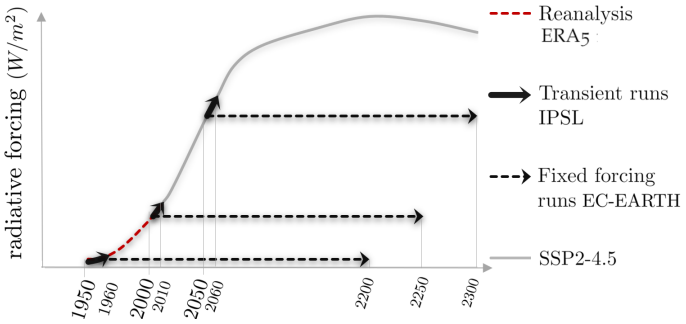

FIG. 2. Schematic of the simulations and the corresponding historical/scenario radiative forcing applied.

B. METHODS

In the first part (Sect. III.A), we assess the performance of the models by comparing the climatology in observations with that of the Present-day simulations. We use monthly data and evaluate (i) zonal-mean temperature (Tzm), in order to determine the lower- and upper-level meridional temperature gradients and the position of the tropopause, (ii) zonal-mean zonal wind (Uzm), to determine the vertical structure of the jet streams, (iii) zonal wind at 200hPa (U200) to identify the horizontal structure of the jet streams, and (iv) sea level pressure (SLP) to compare the climatological high and low pressure systems.

In the second part (Sect. III.B), we evaluate the changes in the climatological large-scale atmospheric circulation of the two models as a function of the radiative forcing applied: Present-minus-Past, Future-minus-Present, and Future-minus-Past. We make use of monthly data and analyse changes in Tzm, SLP and U200. Then, we explore the cause of those changes by computing differences in the zonal asymmetries of geopotential height at 200hPa (Z* 200) and the vertically-averaged zonal wind between 850hPa and 700hPa. We also make use of daily data at 500hPa for assessing changes in the eddy-mean flow interaction. We compute and compare the eddy momentum flux, $\overline{u'v'}$, and the eddy heat flux, $\overline{v'T'}$, where the over-bars denote a time average (in this case, seasonal means) and the primes indicate temporal anomalies of high frequency, here estimated using the 24-hour filter (*Wallace et al.* 1988).

Statistical significance is assessed with a Student's t-test for difference of means at the 95% confidence level.

III. RESULTS

A. Present atmospheric state: simulations versus observations

We first evaluate the present-day radiative forcing simulations with observational data. Figure 3 shows the DJF

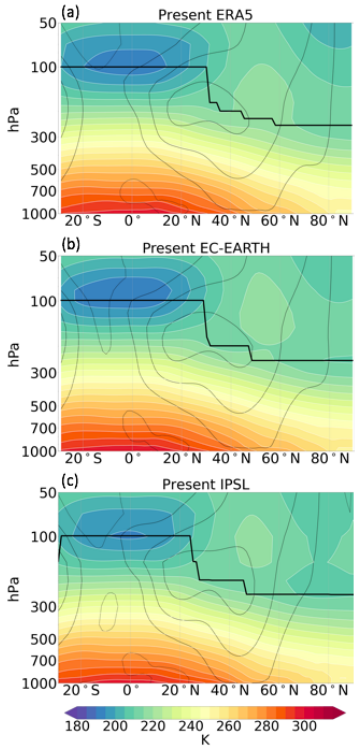

FIG. 3. Vertical cross-section of zonal-mean temperature (shading) and zonal wind (thin black contours every 10 m/s) averaged over the North Atlantic [80W,20E] for: (a) ERA5 reanalysis, (b) EC-EARTH and (c) IPSL. The thick black contour stands for the tropopause, determined using the World Meteorological Organization (WMO) tropopause definition (*Maddox and Mullendore* 2018) as the first height where the atmospheric lapse rate is less than 2 K km^{-1}.

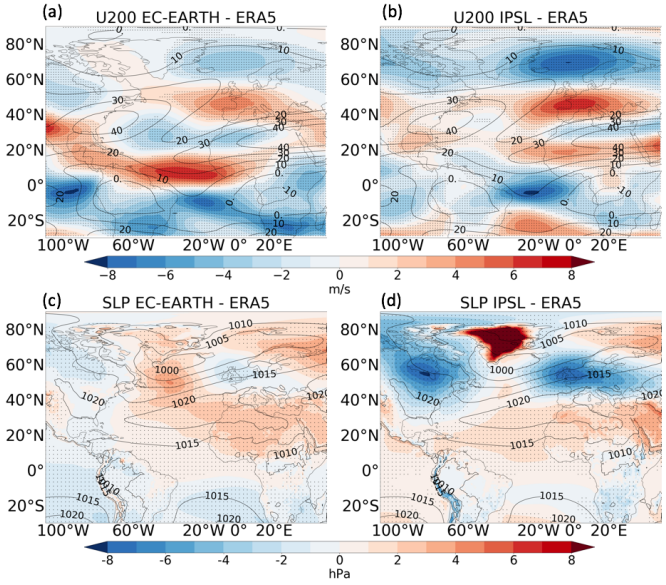

FIG. 4. Model bias, with respect to ERA5, in EC-EARTH (left column) and IPSL (right column) of (a,b) zonal wind at 200hPa and (c,d) sea level pressure. ERA5 climatology is shown in contours (m/s for (a,b), hPa for (c,d)). Dots indicate statistically significant areas.

zonal-mean temperature (shading) and zonal wind (thin contours), averaged over the North Atlantic basin, for ERA5 (top row), EC-EARTH (middle row) and IPSL (bottom row). Both models properly simulate the meridional temperature gradient in the troposphere, as found in reanalysis. They also capture the distinctive structure of the mean flow, yielding the baroclinic jet (or subtropical jet), which has easterlies at low levels and westerlies aloft, and the barotropic jet (or eddy-driven jet), which has westerlies throughout the vertical column. The subtropical jet has its maximum at about 30°N and 200hPa, while the eddy-driven jet maximum is located at 50°N and 200hPa approximately.

Regarding the horizontal structure of the zonal wind at 200hPa (Fig. 4a,b), both models show a positive bias over southern Europe and a negative bias over the Norwegian Sea and northern Europe, with respect to reanalysis. Such systematic deviations reveal a more zonal, less tilted, North Atlantic eddy-driven jet, particularly at its exit region. This is a common error in climate models (e.g. CMIP3 - *Woollings and Blackburn* 2012; CMIP5 - *Zappa et al.* 2013; CMIP6 - *Simpson et al.* 2020), where some meso-/synoptic-scale processes, such as diabatic heating, orography or dissipation, are not well resolved; parameterizations and model formulation are also contributing factors. The bias in upper-level zonal wind is also reflected at lower levels, in the SLP climatology (Fig. 4c,d), with overestimated surface pressure over the North African-Mediterranean region and northern Europe and underestimated over central Europe.

B. Atmospheric response under different radiative forcings

In this section, we analyse the changes in the mean atmospheric state as a function of the radiative forcing, from Past to Future. First, we show changes in the zonal-mean temperature over the North Atlantic basin (Fig. 5), which can modulate baroclinicity as explained in the Introduction. From Past to Present, both models show a weak warming of the troposphere (Fig. 5a,d). This warming is more pronounced below 700hPa at high latitudes and above 500hPa in the tropics, which can be interpreted as a first signature of the AA and UTW, respectively. In IPSL, the tropopause expands in latitude associated with the tropospheric warming (Fig. 5d), likely due to thermal expansion; this is less pronounced in EC-EARTH (Fig. 5a). Larger differences are found between the Future and Present states (Fig. 5b,e), where both the UTW and AA are more evident. EC-EARTH shows a stronger warming than IPSL at all latitudes. In this case, EC-EARTH depicts a clear thermal expansion of the troposphere, including an increase in the tropopause height (Fig. 5b). A similar but larger response is obtained when

comparing Future with respect to Past conditions (Fig. 5c,f), which together suggests that the atmospheric temperature response to radiative forcing scales linearly with the amplitude of the forcing applied.

If the zonal-mean average is computed globally (not shown), instead of regionally over the North Atlantic (Fig. 5), the results largely remain unchanged, apart from a slight confinement of the AA towards higher latitudes in the regional average. This reduction in the latitudinal extent of the AA, particularly noticeable in Future-minus-Present and Future-minus-Past, could be explained by the "warming hole" over the North Atlantic subpolar gyre, namely a *relative* cooling south of Iceland (see Figs. 10 and 15 below). This "warming hole" has been linked to a weakening of the AMOC with increasing radiative forcing (*Drijfhout et al.* 2012).

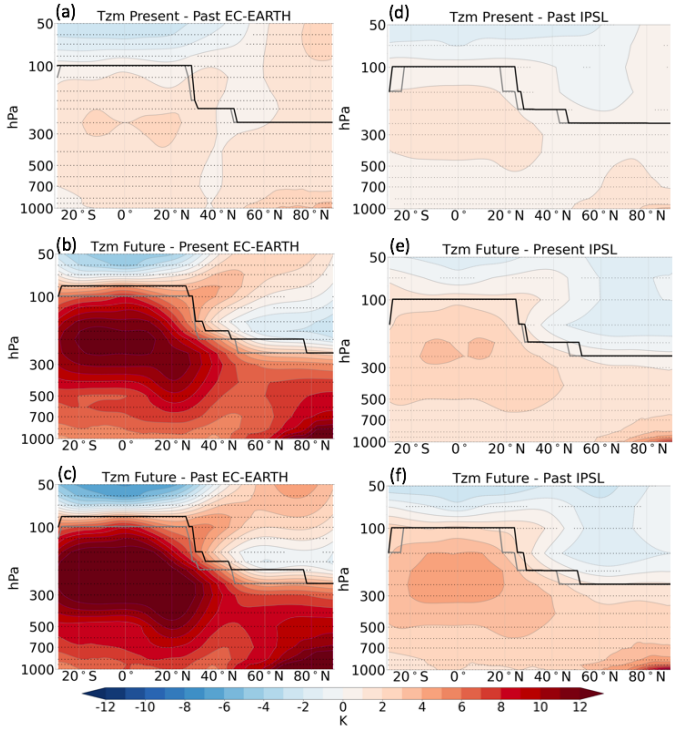

FIG. 5. Vertical cross-section of zonal-mean temperature averaged over the North Atlantic (as in Fig. 3) for Present-minus-Past (top row), Future-minus-Present (middle row), and Future-minus-Past (bottom row) differences in (a,b,c) EC-EARTH and (d,e,f) IPSL. The thick black (grey) contour corresponds to the tropopause of the addend (subtracting) period. Dots indicate statistically significant areas.

Figure 5 highlights that the forced changes in EC-EARTH are larger in amplitude than in IPSL, which may reflect the contrast between experiments. While EC-EARTH simulations consist of 240-year integrations with fixed radiative forcing, IPSL simulations are 24-member ensembles of transient runs; so that EC-EARTH could be more stabilized to the level of radiative forcing. In addition, the strongest differences appear in the Future state with respect to Present and Past. As shown in Figure 2, the projected Future radiative forcing in the SSP2-4.5 scenario is much higher than the Present and Past radiative forcings, which may contribute to the larger warming in (the *stabilized*) EC-EARTH. Alternatively, the difference in the forced changes between EC-EARTH and IPSL may be due to a different climate sensitivity, which in EC-EARTH has increased from CMIP5 to CMIP6 associated with a more advanced treatment of aerosols (*Wyser et al.* 2020). This distinctive amplitude in EC-EARTH, as compared to IPSL, applies to almost all the fields analysed.

The two left columns in Figure 6 show forced changes in SLP. Present-minus-Past differences (Fig. 6a,b) show a decrease of surface pressure in both models over the eastern coast of North America, extending eastward from Newfoundland, and also in the tropical Atlantic over Africa. The most prominent signals appear in the Future state (Fig. 6e-f,i-j): both models display two anomalous low-pressure centres straddling the equator and centred around 20°W; at mid-latitudes, they show an increase in SLP over the Mediterranean region; and at polar latitudes, over the Hudson Bay and spreading out to the Labrador Sea, there is a consistent reduction of SLP.

The two right columns in Figure 6 show forced changes in zonal wind at 200hPa. A consistent tripolar pattern is found in the Present-minus-Past differences (Fig. 6c,d), with positive (i.e. westerlies) anomalies over the southward flank of the North Atlantic-jet's entrance region, accompanied by negative (i.e. easterlies) anomalies at lower and higher latitudes. In the Future scenario these differences generally increase in amplitude, and the anomalous westerly flow extends eastward into Europe (Fig. 6 g-h,k-l). In EC-EARTH, the strengthening of the response in the tropical-subtropical Atlantic is located at the same longitude (approximately 40°W). At high latitudes, EC-EARTH shows maximum negative anomalies south of Greenland while in IPSL they are centred slightly polewards, over land.

As for temperature (Fig. 5) and the variables analysed in Figure 6, the magnitude of the response under Future radiative forcing of all the fields analysed is much stronger than under the other two radiative forcings. As they appear to scale, in the following we only show Present-minus-Past and Future-minus-Present differences. The figures for Future-minus-Past are included in the Appendix.

Thermally-driven versus eddy-driven effects

To explore the causes of the forced changes in the mean atmospheric state described in the previous section, we distinguish between thermally-driven and eddy-driven dynamical patterns (*Gervais et al.* 2019, *Hoskins and Karoly* 1981). The thermally-driven response is characterized by a baroclinic vertical structure, with fields having opposite sign at lower and upper levels. This response usually involves convergence (divergence) at lower

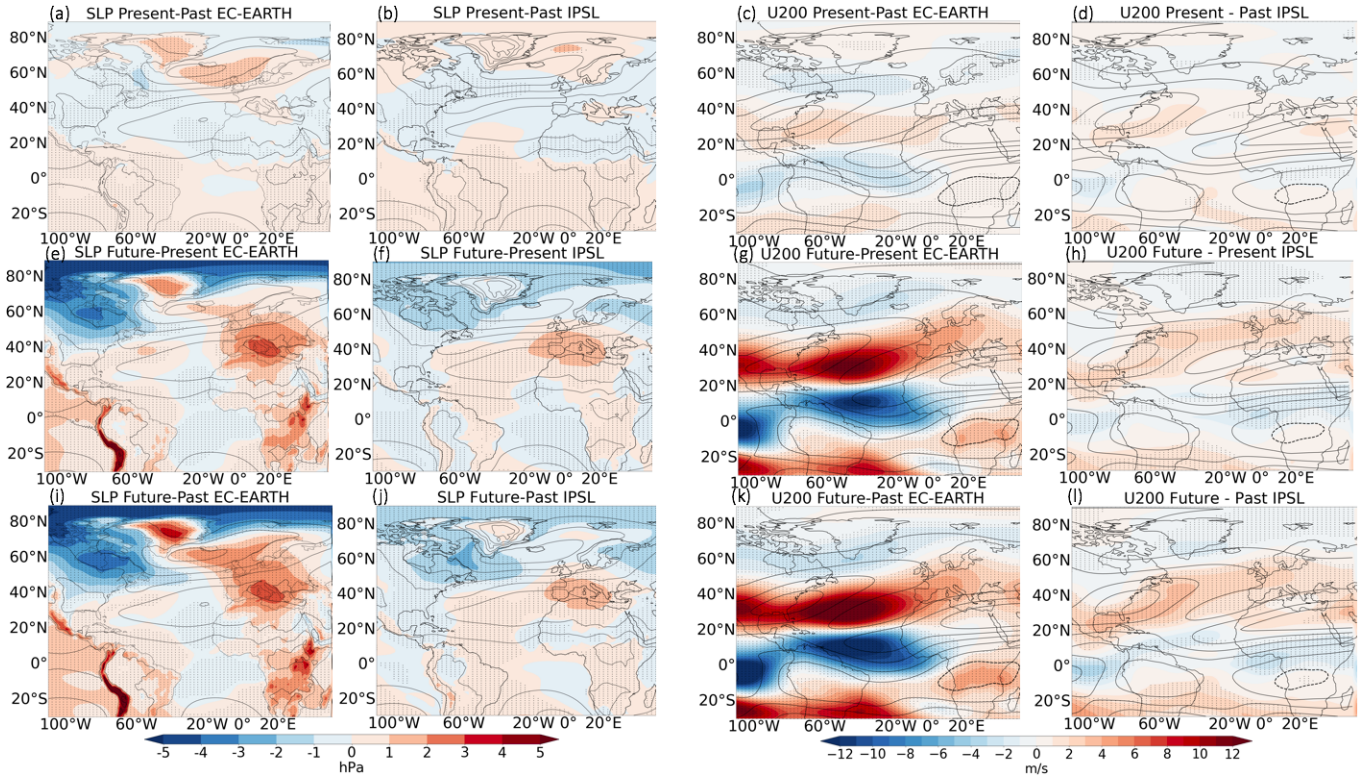

FIG. 6. Present-minus-Past (top row), Future-minus-Present (middle row), and Future-minus-Past (bottom row) differences of sea level pressure in EC-EARTH (a,e,i) and IPSL (b,f,j), and zonal wind at 200hPa in EC-EARTH (c,g,k) and IPSL (d,h,l). Contours stand for the climatology of the subtracting period, that is, Past in the top and bottom rows and Present in the middle row (same contour interval as in Fig. 4; dashed contours indicate negative values). Dots indicate statistically significant ares.

levels and divergence (convergence) at upper levels. On the other hand, where fields have the same sign in the vertical, the response depicts a barotropic structure, pointing to a larger contribution from eddy-driven effects.

In order to distinguish the different mechanisms at play, thermally-driven or eddy-driven, we first compute the differences in geopotential height at 200hPa (Fig. 7, two left columns; Fig. 11) and compare it with those in SLP (Fig. 6, two left columns). In order to filter the radiatively-forced thermal expansion of the forced signal, which mainly depends on latitude (discussed in Fig. 5), and concentrate on the dynamical response, zonal asymmetries in geopotential height with respect to its zonal-mean have been analysed (Fig. 7a-b,e-f). In response to radiative forcing, two anticyclonic anomalies over the tropical Atlantic straddling the equator are present in EC-EARTH, stronger in Future-minus-Present (Fig. 7e) than in Present-minus-Past (Fig. 7a). They are also present in IPSL in the total geopotential height field (Fig. 11d-f in the Appendix), but they are masked in the zonal-eddy field (Fig. 7b,f) because there are stronger anomalies in the zonal-mean over the Indian Ocean (not shown). The pair of off-equatorial anticyclones at upper levels are located approximately over the two symmetric cyclonic anomalies of SLP (Fig.6a-b,e-f), revealing a baroclinic pattern reminiscent of the well-known Gill-type response (*Gill* 1980) to a diabatic heating source (see precipitation differences in Fig. 8 below, as a proxy of the anomalous diabatic heating). At mid-latitudes, both models show an anomalous anticyclonic circulation over the Mediterranean region in Future-minus-Present (Fig. 7e,f), also seen but weaker in Present-minus-Past (Fig. 7a,b). In the previous section, we found an anomalous high pressure system over the same region at low levels (Fig. 6a-b,e-f), thus yielding a barotropic pattern likely caused by eddy-mean flow interaction, particularly strong in the Future state. Another consistent signal between the two models in the Future state is the anomalous cyclonic circulation south of Greenland (Fig. 7e,f). Again, such upper-level anomaly has the same sign as that of surface pressure (Fig. 6e,f), depicting a barotropic pattern, where eddy effects are also expected. On the contrary, over the Hudson Bay in IPSL and west of Greenland in EC-EARTH, that is upstream of the cyclonic circulation at subpolar latitudes, a baroclinic pattern is found, with positive anomalies at 200hPa (Fig. 7e,f) and negative anomalies of SLP (Fig. 6e,f). This thermally-driven structure might be associated with a thermal-low effect in response to sea-ice reduction (see Fig. 10 below): the ascending warmer air leads to negative pressure anomalies

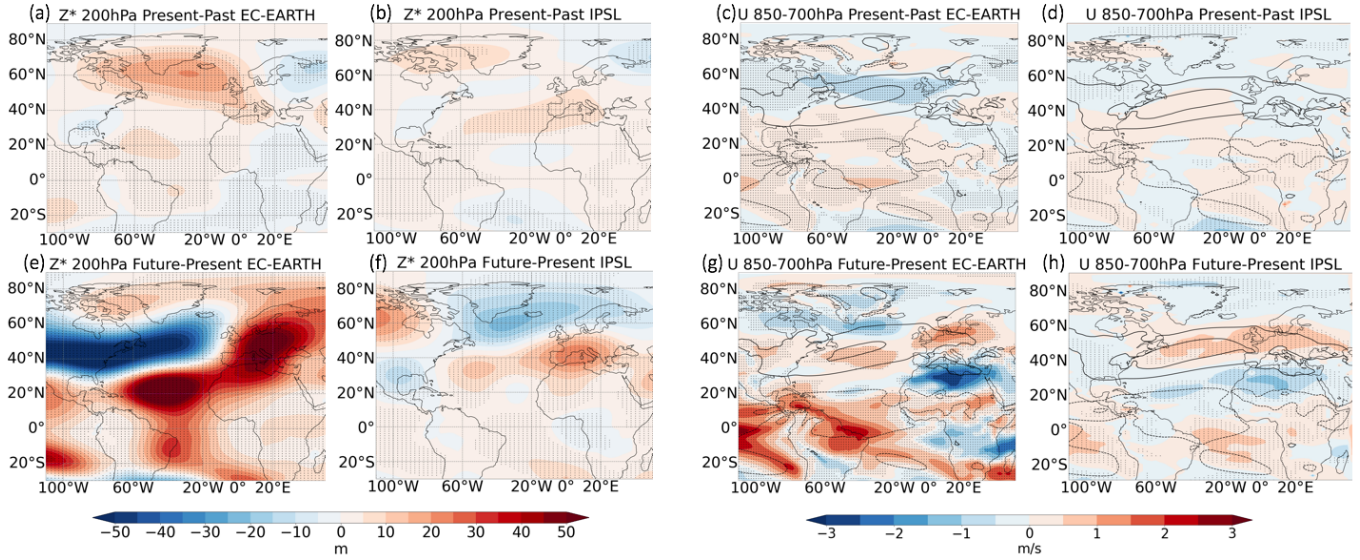

FIG. 7. Present-minus-Past (top row) and Future-minus-Present (bottom row) differences of geopotential height zonal asymmetries at 200hPa in EC-EARTH (a,e) and IPSL (b,f), and zonal wind vertically averaged from 850hPa to 700hPa in EC-EARTH (c,g) and IPSL (d,h). Contours stand for the climatology of the subtracting period, that is, Past in the top row and Present in the bottom row (contour interval every 5 m/s from -5 m/s to 10 m/s; dashed contours indicate negative values). Dots indicate statistically significant areas.

at lower levels and positive geopotential height anomalies at upper levels caused by thermal expansion (e.g. *Chripko et al.* 2021, *Osborne et al.* 2017), although other mechanisms may also be operating (e.g. *Deser et al.* 2004, *Hoskins and Karoly* 1981). This high-latitude baroclinic response is also noticeable in Present-minus-Past, albeit weaker (Figs. 6a-b, 7a,b).

Because the eddy-driven jet is barotropic in structure, we use zonal wind at low levels, vertically averaged from 850hPa to 700hPa (Fig. 7 two right columns), as a diagnostic to asses forced changes in the eddy-driven jet. In Present-minus-Past (Fig. 7c,d), only EC-EARTH shows statistically significant positive anomalies southward of the eddy-driven jet entrance and negative anomalies at the eddy-driven jet core and exit, although they are relatively weak. In Future-minus-Present, the differences are much more significant and stronger in both models, and more consistent between them (Fig. 7g,h). At low latitudes, anomalous 200hPa westerlies at the entrance of the North Atlantic jet and easterlies equatorward of it were found (Fig. 6g,h), but these anomalies are not evident at lower levels. The baroclinic structure of such anomalies, with anomalous westerlies around the equator (Fig. 7g,h), confirms their thermal origin as part of the Gill-type response discussed above (Fig. 7e,f). At mid-latitudes, in both models there is a strengthening of the westerly flow into northern Europe at lower and upper levels. In addition, there are anomalous easterlies south of the Mediterranean basin (Fig. 7g,h), linked to the barotropic anticyclonic circulation in this region (Figs. 6e-f, 7e-f). Likewise, the lower-level easterly anomalies over Greenland (Fig. 7g,h) are consistent with the barotropic cyclonic circulation found at high latitudes (Figs. 6e-f, 7e-f), with anomalous easterlies at upper levels (Fig. 6g,h).

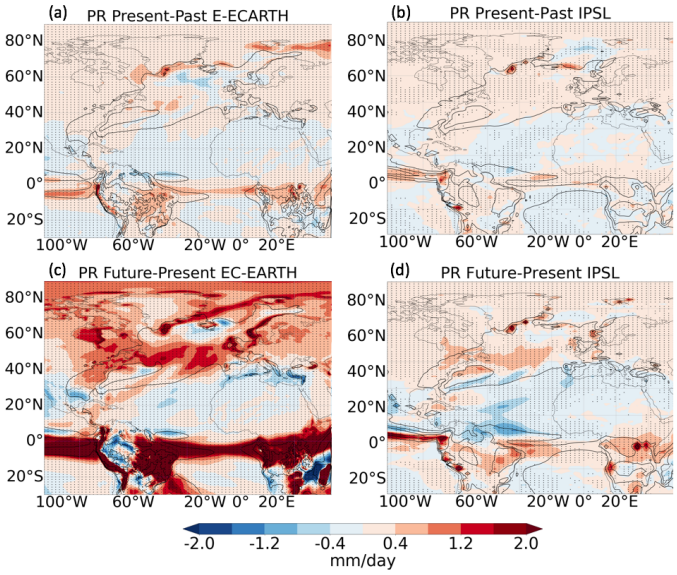

FIG. 8. Present-minus-Past (top row) and Future-minus-Present (bottom row) differences of precipitation in EC-EARTH (a,c) and IPSL (b,d). Contours stand for the climatology of the subtracting period, that is, Past in the top row and Present in the bottom row (contour interval 3 mm/day from 3mm/day to 9mm/day). Dots indicate statistically significant areas.

Figure 8 shows forced changes in total precipitation. It accounts for both stratiform or large-scale precipitation

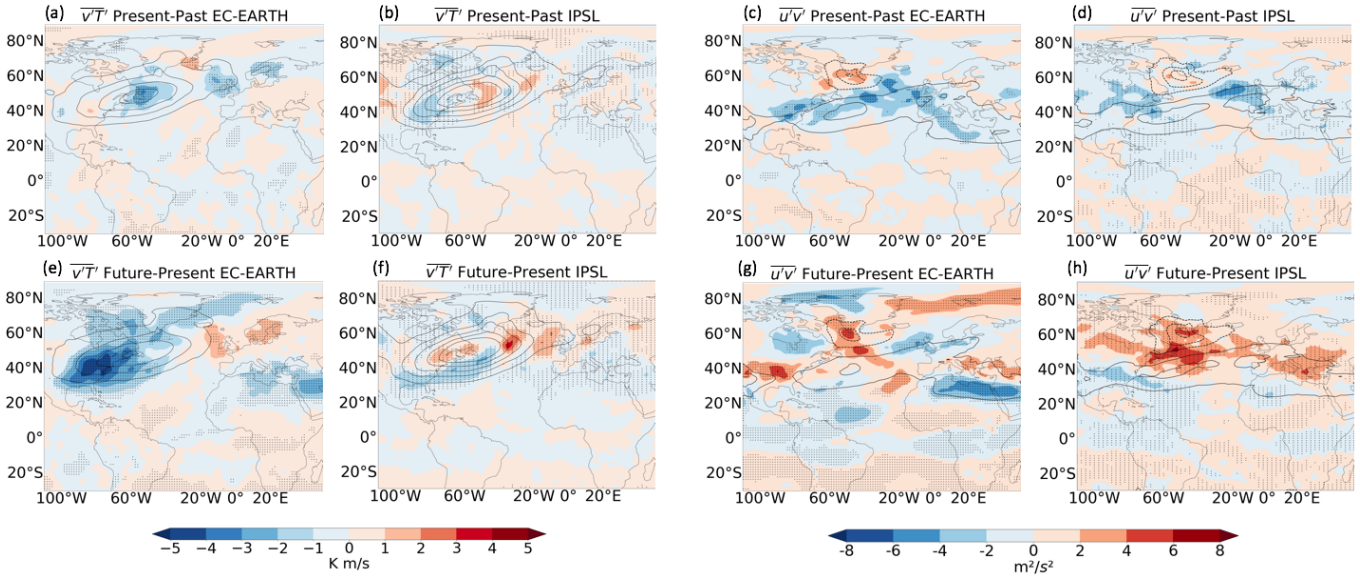

FIG. 9. Present-minus-Past (top row) Future-minus-Present (bottom row) differences of $\overline{v'T'}$ at 500hPa in EC-EARTH (a,e) and IPSL (b,f), and $\overline{u'v'}$ at 500hPa in EC-EARTH (c,g) and IPSL (d,h). Contours stand for the climatology of the subtracting period, that is, Past in the top row and Present in the bottom row (contour interval of $\overline{v'T'}$ every 5 K m/s from 5 K m/s to 25 K m/s, and $\overline{u'v'}$ every 10 m^2/s^2 from -20 m^2/s^2 to 30 m^2/s^2; dashed contours indicate negative values). Dots indicate statistically significant areas.

and convective precipitation. In order to interpret these differences, they can be decomposed by their origin: thermodynamical, related to moisture changes, or dynamical, related to atmospheric circulation changes (*Collins et al.* 2013). In Present-minus-Past (Fig. 8a,b), both models show a weak intensification of the Intertropical Convergence Zone (ITCZ). This may probably result from the thermodynamical component: an increase in moisture at lower levels associated with an increase in temperature, leading to more condensation in the deep convection (see Introduction). At tropical-subtropical latitudes, there is a decrease in precipitation likely due to the increase in deep convection and the related outflow and subsidence; although an increase in static stability, as a result of the increase in temperature in the middle-upper troposphere, could also play a role. At mid-latitudes, there is a weak increase north of the maximum storm-track precipitation, which has been suggested to be primarily caused by thermodynamical effects (*Emori and Brown* 2005), due to large positive temperature anomalies over this region (see Fig. 10). In Future-minus-Present (Fig. 8c,d), these differences are overall reinforced. Note that the increase in precipitation near the equator, linked to the intensified ITCZ, would reflect the increase in diabatic heating responsible for the Gill-type response discussed above. The dry conditions over the Mediterranean region are consistent with the anomalous anticyclonic circulation found there (Figs. 6e-f, 7e-f), while the wet conditions over northern Europe are probably associated with the strengthening of the westerly winds into Europe (Figs. 6g-h, 7g-h).

In order to asses the eddy-mean flow interaction, and to analyse to what extent the radiatively-forced changes involve synoptic-scale wave activity, the eddy covariances $\overline{u'v'}$ and $\overline{v'T'}$ at 500hPa have been computed (Fig. 9). They are proportional to the meridional and vertical components of the Eliassen-Palm flux, respectively. They provide information of wave propagation and its divergence measures the eddy-mean flow interaction (*Edmon et al.* 1980). $\overline{u'v'}$ denotes the transient-eddy momentum flux, being positive (negative) when the eddies transport westerly momentum northward (southward). If the transient-eddy momentum flux converges, the synoptic-scale waves act to accelerate the mean flow, while if it diverges, they act to decelerate the mean flow. $\overline{v'T'}$ denotes the transient-eddy heat flux, being positive (negative) when the eddies transport heat northward (southward). It is also a measure of vertical wave propagation, with positive values indicating upward propagation of wave activity.

Figure 9 (two left columns; contours) shows the climatology of $\overline{v'T'}$, with the maximum coinciding with the largest meridional temperature gradient, which is the main source region of baroclinic activity. Figure 9 (two right columns; contours) shows the climatology of $\overline{u'v'}$, with the maximum located downstream the maximum of $\overline{v'T'}$: there is a positive band at middle latitudes and a negative band at subpolar latitudes, converging momentum at around 50°N, which is the region of the eddy-driven jet (e.g. *Vallis and Gerber* 2008).

In Present-minus-Past, both models show negative $\overline{u'v'}$ anomalies along the climatological positive band and positive $\overline{u'v'}$ anomalies over the climatological negative centre south of Greenland (Fig. 9c,d). Hence, the eddies are

weakening the eddy-driven jet (cf. Figs. 6c-d, 7c-d). In Future-minus-Present, both models display a reinforcement of the positive anomalies south of Greenland (Fig. 9g,h), illustrating that barotropic processes are at play. They also show negative anomalies over northern Africa and positive anomalies over south-eastern Europe. Thus, over the Mediterranean, there is anomalous divergence of momentum, supporting the hypothesis that eddy activity is extracting momentum from the mean flow over this region and depositing it over central Europe, accelerating the mean flow there and extending the eddy-driven jet eastward (cf. Fig. 7g,h). Consistently, in Future-minus-Present there are positive $\overline{v'T'}$ anomalies over western Europe (Fig. 9e,f), pointing out enhanced wave activity in this region. These results are in agreement with previous studies (*Woollings et al.* 2012, *Zappa et al.* 2012).

In the western North Atlantic, both models show an overall reduction in $\overline{v'T'}$ with increasing radiative forcing, which becomes stronger in Future climate: in EC-EARTH over its climatological maximum (Fig. 9a,e) and in IPSL poleward and equatorward of its climatological maximum (Fig. 9b,f). This reduction in baroclinic processes is possibly a consequence of the reduced meridional temperature gradient associated with the warming at high latitudes (Fig. 10), whereby linked to a reduced poleward heat flux.

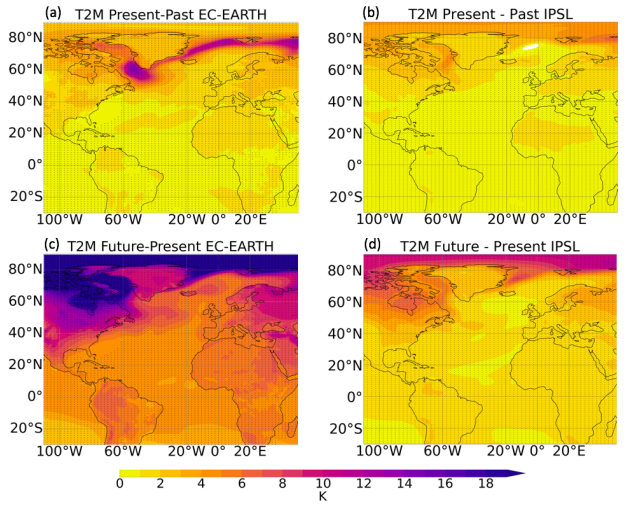

FIG. 10. Present-minus-Past (top row), Future-minus-Present (bottom row) differences of air temperature at 2 metres in EC-EARTH (a,c) and IPSL (b,d). Dots indicate statistically significant areas.

IV. CONCLUSIONS

In this work, we have not thoroughly evaluated the performance of the models to simulate the observed atmospheric circulation climatology, but used two different approaches to isolate the radiatively-forced changes in atmospheric circulation, from past to future levels of radiative forcing, from internal variability. Hence, we have emphasized the consistent signals between the two approaches, which are summarized as follows:

1) Both approaches yield a forced response that increases in amplitude from Present-minus-Past to Future-minus-Present. EC-EARTH generally shows a stronger amplitude in those differences, probably because of a higher climate sensitivity and an experimental set-up where the model is stabilized to the fixed radiative forcing. IPSL is continuously in a transient state and it is not adjusted to the radiative forcing.

2) At low latitudes, in the tropical Atlantic, the forced atmospheric response is characterized by a Gill-type baroclinic structure, where the anomalous anticyclonic circulation at upper levels reinforces the westerly wind at the equatorward flank of the North Atlantic jet.

3) At high latitudes, the forced response is reminiscent of the 'Arctic Amplification' linked to sea-ice reduction, and a thermally-driven baroclinic structure can be seen over the Hudson Bay (IPSL) and west of Greenland (EC-EARTH).

4) At mid-latitudes, the forced response shows a barotropic pattern, with a cyclonic (anticyclonic) circulation in the North Atlantic (Euro-Mediterranean) sector, suggesting a role for eddy-related effects. These circulation anomalies are associated with a decrease in precipitation over the Mediterranean and an increase over central Europe. Changes in transient-eddy activity are consistent with a strengthening and eastward extension of the eddy-driven jet, and with a decrease in zonal wind over the Mediterranean and northern Africa.

Due to the complexity of the thermodynamical and dynamical factors that modulate the North Atlantic atmospheric circulation, further research is needed to confirm our findings. An interesting prospect envisaged from this work is the use of the recently-developed Large Ensembles of climate simulations, such as the one performed with IPSL-CM6, to try isolating *ad-hoc* the forced response to a particular level of radiative forcing instead of having to run targeted simulations with a fixed radiative forcing, which is very costly, such as those performed with EC-EARTH. More research on the storm-track activity would allow a better understanding of its contribution to the mean-flow changes. For example, a Lagrangian approach, making use of 6-hourly data, could be used to track individual cyclones and determine changes in their intensity and frequency.

ACKNOWLEDGMENTS

I would like to express my deep and sincere gratitude to my two supervisors, Javier García Serrano and Guillaume Gastineau, for the valuable guidance, for giving me the opportunity to do research and for being a great inspiration. I am also thankful to my master's colleagues for sharing good moments and stimulating discussions during the course. Finally, I am extremely grateful to

my parents and sister for being constant supporters.

REFERENCES

Boucher, O., et al., Presentation and evaluation of the IPSL-CM6A-LR Climate Model, *Royal Meteorological Society*, *12*, doi:10.1029/2019MS002010, 2020.

Brayshaw, D., et al., The basic ingredients of the North Atlantic storm track. part i: Land–sea contrast and orography, *J. Atmos. Sci.*, *66*, 2539–2558, doi:10.1175/2009JAS3078.1, 2009.

Chripko, S., et al., Impact of reduced arctic sea ice on northern hemisphere climate and weather in autumn and winter, *J. Climate*, *34*, 5847–5867, doi:10.1175/JCLI-D-20-0515.1, 2021.

Collins, M., et al., Long-term climate change: Projections, commitments and irreversibility, 2013.

Deser, C., et al., The effects of North Atlantic SST and sea ice anomalies on the winter circulation in CCM3. Part II: Direct and indirect components of the response, *J. Clim.*, *17*, 877–889, 2004.

Deser, C., et al., Uncertainty in climate change projections: the role of internal variability, *Clim Dyn*, *38*, 527–546, doi:10.1007/s00382-010-0977-x, 2012.

Deser, C., et al., Insights from Earth system model initial-condition large ensembles and future prospects, *Nat. Clim. Chang.*, *10*, 277–286, doi:10.1038/s41558-020-0731-2, 2020.

Drijfhout, S., et al., Is a decline of AMOC causing the warming hole above the North Atlantic in observed and modeled warming patterns?, *Journal of Climate*, *25*, doi:10.1175/JCLI-D-12-00490.1, 2012.

Edmon, H., et al., Eliassen-palm cross sections, *J. Atmos. Sci.*, *37*, 2600–2616, doi:10.1175/1520-0469(1980)037¡2600:EPCSFT¿2.0.CO;2, 1980.

Emori, S., and S. Brown, Dynamic and thermodynamic changes in mean and extreme precipitation under changed climate, *Geophysical Research Letters*, *32*, doi:10.1029/2005GL023272, 2005.

Gervais, M., et al., Impacts of the North Atlantic Warming Hole in future climate projections: Mean atmospheric circulation and the north atlantic jet, *J. Clim.*, *32*, 2673–2689, doi:10.1175/JCLI-D-18-0647.1, 2019.

Gill, A. E., Some simple solutions for heat-induced tropical circulation, *Royal Meteorological Society*, *106*, 447–462, doi:10.1002/qj.49710644905, 1980.

Hersbach, H., et al., The ERA5 global reanalysis, *Royal Meteorological Society*, *146*, 1999–2049, doi:10.1002/qj.3803, 2020.

Holton, J. R., *An Introduction to Dynamic Meteorology*.

Hoskins, B. J., and D. J. Karoly, The steady linear response of a spherical atmosphere to thermal and orographic forcing, *J. Atmos. Sci.*, *38*, 1179–1196, 1981.

Houghton, J., et al., *Climate Change 2001: The Scientific Basis*, 2001.

Maddox, E., and G. Mullendore, Determination of best tropopause definition for convective transport studies, *J. Atmos. Sci.*, *75*, 3433–3446, doi:10.1175/JAS-D-18-0032.1, 2018.

Meinshausen, M., et al., The shared socio-economic pathway (SSP) greenhouse gas concentrations and their extensions to 2500, *Geosci. Model Dev.*, *13*, 3571–3605, doi:10.5194/gmd-13-3571-2020, 2020.

O'Neill, B., et al., The Scenario Model Intercomparison Project (ScenarioMIP) for CMIP6, *Geosci. Model Dev.*, *9*, 3461–3482, doi:10.5194/gmd-9-3461-2016, 2016.

Osborne, J., et al., Ocean–atmosphere state dependence of the atmospheric response to arctic sea ice loss, *J. Climate*, *30*, 1537–1552, doi:10.1175/JCLI-D-16-0531.1, 2017.

Serreze, M., and J. Francis, The Arctic Amplification debate, *Climatic Change*, *76*, 241–264, doi:10.1007/s10584-005-9017-y, 2006.

Shaw, T., et al., Storm track processes and the opposing influences of climate change, *Nature Geoscience*, *9*, 656–664, doi:10.1038/ngeo2783, 2016.

Simpson, I., et al., An evaluation of the large-scale atmospheric circulation and its variability in CESM2 and other CMIP models, *Journal of Geophysical Research: Atmospheres*, *125*, doi:10.1029/2020JD032835, 2020.

Vallis, G. K., and E. P. Gerber, Local and hemispheric dynamics of the North Atlantic Oscillation, annular patterns and the zonal index, *Dynamics of Atmospheres and Oceans*, *44*, 184–212, doi:10.1016/j.dynatmoce.2007.04.003, 2008.

Wallace, J., et al., Relationship between cyclone tracks, anticyclone tracks and baroclinic waveguides, *Journal of Atmospheric Sciences*, *45*, 439–462, 1988.

Woollings, T., Dynamical influences on European climate: an uncertain future, *The Royal Society*, doi:10.1098/rsta.2010.0040, 2010.

Woollings, T., and M. Blackburn, The North Atlantic jet stream under climate change and its relation to the NAO and EA patterns, *Journal of Climate*, *25*, 886–902, doi:10.1175/JCLI-D-11-00087.1, 2012.

Woollings, T., et al., Response of the North Atlantic storm track to climate change shaped by ocean–atmosphere coupling, *Nature Geoscience*, *5*, 313–317, 2012.

Wyser, K., et al., On the increased climate sensitivity in the EC-Earth model from CMIP5 to CMIP6, *Geosci. Model Dev.*, *13*, 3465–3474, doi:10.5194/gmd-13-3465-2020, 2020.

Zappa, G., et al., A multimodel assessment of future projections of North Atlantic and european extratropical cyclones in the CMIP5 Climate Models, *J. Clim.*, *26*, 5846–5862, doi:10.1175/JCLI-D-12-00573.1, 2012.

Zappa, G., et al., The ability of CMIP5 models to simulate North Atlantic extratropical cyclones, *Journal of Climate*, *26*, 5379–5396, doi:10.1175/JCLI-D-12-00501.1, 2013.

APPENDIX

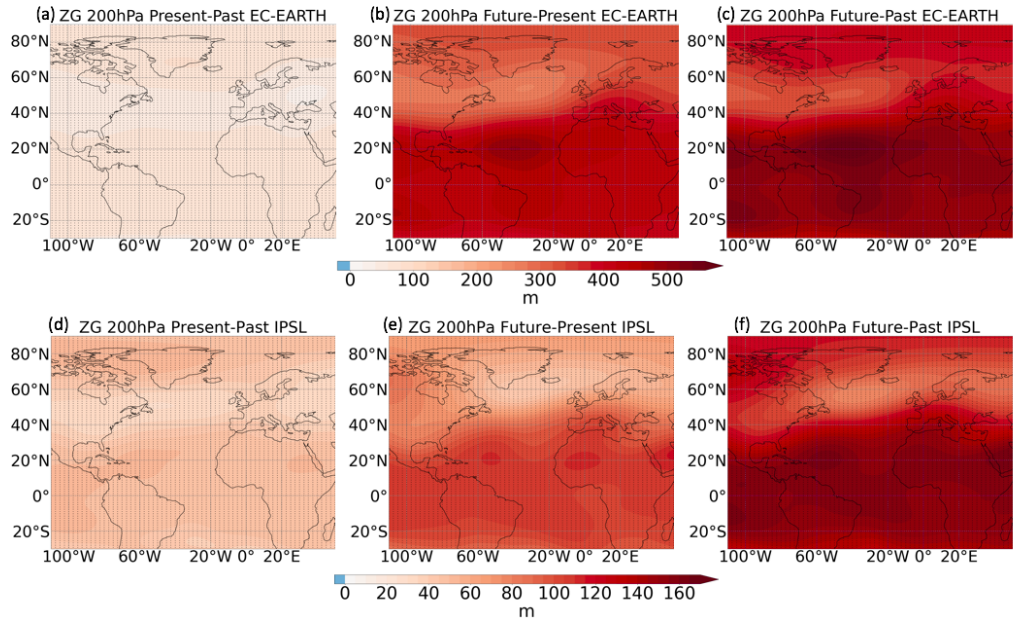

FIG. 11. Present-minus-Past (left), Future-minus-Present (middle), and Future-minus-Past (right) differences of geopotential height at 200hPa in EC-EARH (a,b,c) and IPSL (d,e,f). Note the difference in the colorbars. Dots indicate statistically significant areas.

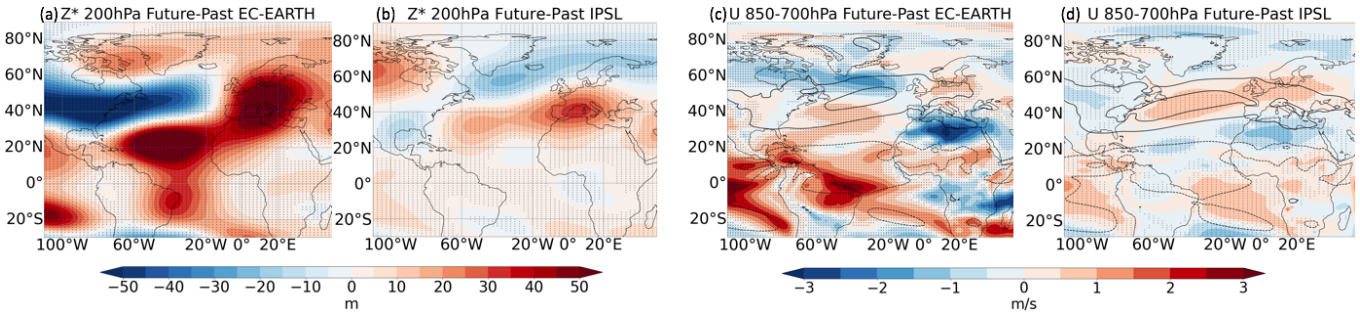

FIG. 12. Future-minus-Past differences of geopotential height zonal asymmetries at 200hPa in EC-EARTH (a) and IPSL (b), and zonal wind vertically averaged from 850hPa to 700hPa in EC-EARTH (c) and IPSL (d). Dots indicate statistically significant areas. Past climate values are shown in contours (contour interval every 5 m/s from -5 m/s to 10 m/s; dashed contours show negative values). Dots indicate statistically significant areas.

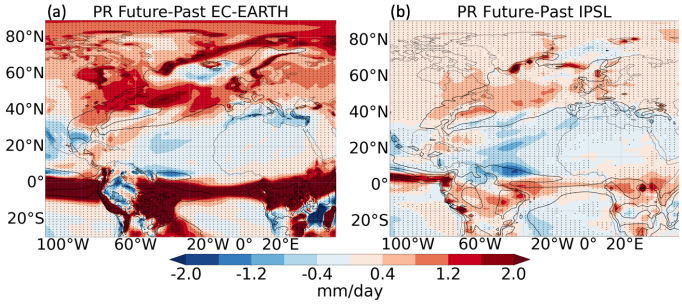

FIG. 13. Future-minus-Past differences of precipitation in EC-EARTH (a) and IPSL (b). Past climate values are shown in contours (contour interval 3 mm/day from 3mm/day to 9mm/day). Dots indicate statistically significant areas.

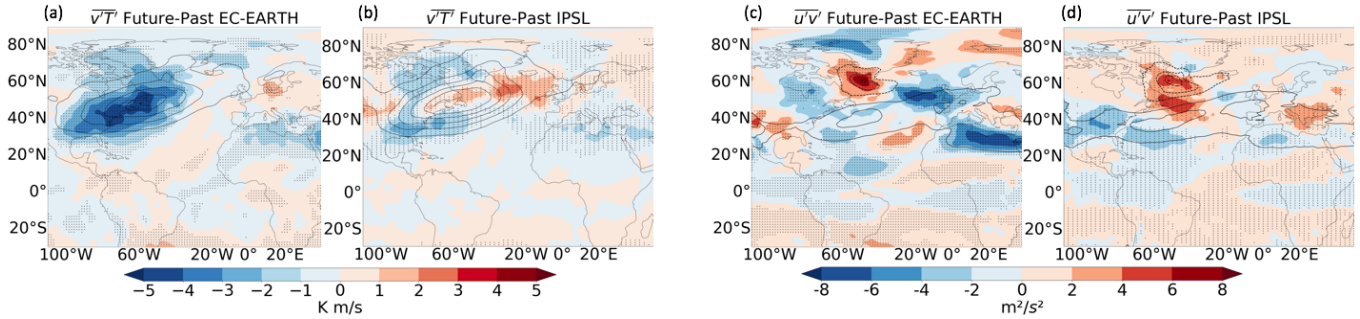

FIG. 14. Future-minus-Past differences of $\overline{v'T'}$ in EC-EARTH (a) and IPSL (b), and $\overline{u'v'}$ in EC-EARTH (c) and IPSL (d). Past climate values are shown in contours (contour interval of $\overline{v'T'}$ every 5 K m/s from 5 K m/s to 25 K m/s, and $\overline{u'v'}$ every 10 m^2/s^2 from -20 m^2/s^2 to 30 m^2/s^2; dashed contours show negative values). Dots indicate statistically significant areas.

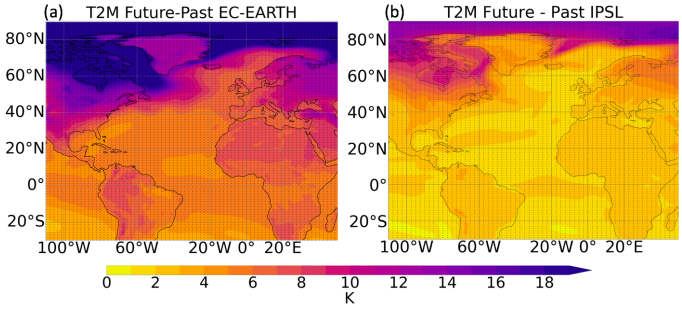

FIG. 15. Future-minus-Past differences of air temperature at 2 metres in EC-EARTH (a) and IPSL (b). Dots indicate statistically significant areas.